The Biochemical Kinetics Underlying Actin Movement Generated by One and Many Skeletal Muscle Myosin Molecules

Josh E. Baker, Christine Brosseau, Peteranne B. Joel, and David M. Warshaw
Department of Molecular Physiology and Biophysics, University of Vermont, Burlington, Vermont 05405 USA

ABSTRACT To better understand how skeletal muscle myosin molecules move actin filaments, we determine the motion-generating biochemistry of a single myosin molecule and study how it scales with the motion-generating biochemistry of an ensemble of myosin molecules. First, by measuring the effects of various ligands (ATP, ADP, and P_i) on event lifetimes, τ_{on}, in a laser trap, we determine the biochemical kinetics underlying the stepwise movement of an actin filament generated by a single myosin molecule. Next, by measuring the effects of these same ligands on actin velocities, V, in an in vitro motility assay, we determine the biochemistry underlying the continuous movement of an actin filament generated by an ensemble of myosin molecules. The observed effects of P_i on single molecule mechanochemistry indicate that motion generation by a single myosin molecule is closely associated with actin-induced P_i dissociation. We obtain additional evidence for this relationship by measuring changes in single molecule mechanochemistry caused by a smooth muscle HMM mutation that results in a reduced P_i-release rate. In contrast, we observe that motion generation by an ensemble of myosin molecules is limited by ATP-induced actin dissociation (i.e., V varies as $1/\tau_{on}$) at low [ATP], but deviates from this relationship at high [ATP]. The single-molecule data uniquely provide a direct measure of the fundamental mechanochemistry of the actomyosin ATPase reaction under a minimal load and serve as a clear basis for a model of ensemble motility in which actin-attached myosin molecules impose a load.

INTRODUCTION

Over thirty years ago, Barany (1967) showed that a muscle's maximum shortening velocity is correlated with its actomyosin ATPase rate, suggesting that myosin's hydrolytic and mechanical processes are coupled. Given that the hydrolysis of ATP by actomyosin is a multi-step biochemical process (Lymn and Taylor, 1971), the challenge over the past several decades has been to characterize the mechanical properties of the individual biochemical states and to determine at what point in its ATPase cycle myosin generates actin movement (i.e., myosin's mechanical step). In an attempt to achieve these goals, various experimental approaches have been used (for reviews see Goldman, 1987; Cooke, 1997; Sellers, 1999), including transient kinetic techniques in solution and mechanical studies in skinned fibers performed simultaneously with spectroscopic (Irving et al., 1995; Baker et al., 1998) or fiber diffraction measurements (Linari et al., 2000). These studies, along with structural data from electron micrographic (Reedy et al., 1965, Taylor et al., 1999) and crystallographic studies (Rayment et al., 1993; Dominguez et al., 1998; Houdusse et al., 2000) suggest the minimal mechanochemical scheme in Fig. 1.

When ATP (T) or the products of hydrolysis, i.e., ADP (D) and inorganic phosphate (P_i), are bound to myosin (M), myosin has a weak affinity for actin (A) and is in, what are referred to as, weak binding states (M·T, M·D·P_i). Upon release of P_i, myosin's affinity for actin increases by several orders of magnitude (White and Taylor, 1976; Eisenberg and Hill, 1985), resulting in strong actin binding (A·M·D) that is maintained even after the release of ADP (A·M). Myosin returns to a weak binding state when an ATP molecule binds to myosin's active site, allowing myosin to detach from actin and to begin its cycle once again.

With the development of the single molecule laser trap assay, direct access to the mechanochemistry of the actomyosin ATPase reaction is now possible (Finer et al., 1994). In this assay, the distance, d, that myosin moves an actin filament can be measured as well as the period of time, t_{on}, that myosin maintains this displacement (Guilford et al., 1997). For smooth and cardiac muscle myosin, changes in the average t_{on}, or lifetime (τ_{on}), with ATP concentration have been used to determine a second-order ATP-induced detachment rate, k_T, and an effective ADP release rate, k_{-D}

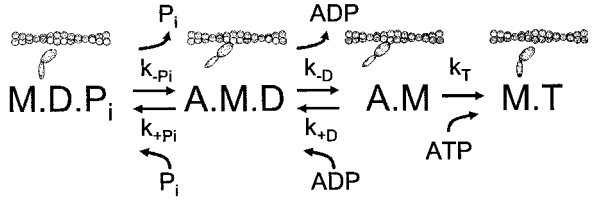

FIGURE 1 A model of the mechanochemistry of the actomyosin ATPase reaction. A myosin head (*ovals*) has a weak affinity for an actin filament (*helix*) when ATP or ADP and inorganic phosphate, P_i, are bound to myosin. Upon P_i release, myosin's affinity for actin increases by several orders of magnitude and, upon strong binding to actin, undergoes a conformational change (a light chain domain rotation). Myosin remains strongly bound to actin even after ADP release.

Submitted October 3, 2001, and accepted for publication November 27, 2001.

Address reprint requests to David M. Warshaw, Dept. of Molecular Physiology and Biophysics, Univ. of Vermont, Burlington, VT 05405. Tel.: 802-656-4300; Fax: 802-656-0747; E-mail: warshaw@physiology.med.uvm.edu.

0006-3495/02/04/2134/14 $2.00

(Lauzon et al., 1998; Palmiter et al., 1999). In the present study, we use a laser trap to estimate values for k_T, k_{-D}, k_D (the second-order ADP binding rate), and k_{Pi} (the second-order P_i-induced actin dissociation rate) for skeletal muscle myosin at the level of a single molecule.

Myosin's mechanical step is believed to result from a discrete rotation of the myosin light chain domain, or neck (Rayment et al., 1993; Dominguez et al., 1998; Baker et al., 1998; Houdusse et al., 2000), with the neck presumably acting as a lever that amplifies small structural changes in the motor domain upon strong actin binding (Uyeda et al., 1996; Anson et al., 1996; Warshaw et al., 2000; Ruff et al., 2001). However, the timing of the mechanical step relative to P_i release remains unclear. Does the mechanical step occur prior to (Dantzig et al., 1992), concomitant with (Eisenberg and Hill, 1985), or after P_i release? Here, we address this question by determining how τ_{on} is affected by $[P_i]$ and by a smooth muscle heavy meromyosin (HMM) mutation that dramatically reduces the actin-activated P_i release rate (Joel et al., 2001).

Finally, in the past, our laboratory (Harris and Warshaw, 1993) and others (Homsher et al., 1993) have used actin filament velocities, V, measured in an in vitro motility assay as a means of estimating actomyosin detachment kinetics by assuming the relationship $V \sim \bar{d}/\tau_{on}$ (Huxley, 1990). This relationship predicts that changes in ligand concentrations that alter single molecule kinetics (i.e., change τ_{on}) should similarly affect V in a motility assay. Implicit in this relationship is the assumption that actin-attached myosin heads in a motility assay impose a load that fully limits actin movement without affecting the detachment kinetics measured in a minimally loaded laser trap assay. In the present study, we test this hypothesis by performing motility assays that parallel our laser trap studies. We observe that, under certain conditions, V measured in a motility assay equals $\bar{d}/\tau_{on}$ determined at the single molecule level, but that at physiological ATP concentrations, V is considerably faster than $\bar{d}/\tau_{on}$. To better understand these data, we develop a simple model in which myosin's mechanical step is partitioned between moving an actin filament and stretching internal compliant linkages in the actomyosin system. This model serves as a framework within which single molecule and ensemble data can be formally compared.

MATERIALS AND METHODS

Proteins

Fast skeletal muscle myosin was prepared from chicken pectoralis as previously described (Warshaw et al., 1990). To investigate how reducing the P_i release rate affects single myosin molecule behavior in the laser trap, a mutant smooth muscle HMM was expressed in which two highly conserved lysines in loop 2 were replaced with alanines (Joel et al., 2001). The kinetics and motile properties of this mutant have been characterized extensively and suggest that the predominant effect of the mutation is to dramatically reduce the rate of actin-activated P_i release (Joel et al., 2001). All myosins were stored in glycerol at −20°C (Warshaw et al., 1990).

Immediately before use in the motility and laser trap assays, myosin was further purified to eliminate "dead heads" by centrifugation with equimolar actin and 1 mM ATP in myosin buffer (see Buffers below). *N*-ethylmaleimide-modified skeletal myosin (NEM-myosin) was prepared as previously described (Warshaw et al., 1990) and was used to bind actin filaments to polystyrene beads (1.0 μm dia. polystyrene; Polysciences Inc., Warrington PA; Guilford et al., 1997). Actin was isolated from chicken pectoralis (Pardee & Spudich, 1982) and incubated overnight with tetramethylrhodamine isothiocyanate (TRITC)-labeled phalloidin as previously described (Warshaw et al., 1990).

Buffers

Myosin buffer (MB) contained 0.3 M KCl, 25 mM imidazole, 1 mM EGTA, 4 mM $MgCl_2$, and 10 mM DTT, adjusted to pH 7.4. Actin buffer (AB) contained 25 mM KCl, 25 mM imidazole, 1 mM EGTA, 4 mM $MgCl_2$, 10 mM DTT, and oxygen scavengers (0.1 mg ml^{-1} glucose oxidase, 0.018 mg ml^{-1} catalase, 2.3 mg ml^{-1} glucose) adjusted to pH 7.4. For experiments in which a range of ligands were tested (i.e., 0.1 μM to 1 mM ATP, 0–5 mM MgADP, and 0–40 mM inorganic phosphate, P_i), the desired ligand concentration was added to AB. To maintain a constant ionic strength and a 3-mM free Mg^{+2} concentration, the KCl and $MgCl_2$ concentrations were adjusted according to an algorithm based on Fabiato and Fabiato (1979).

Laser trap

Detailed protocols for the laser trap assay have been previously described (Dupuis et al., 1997; Guilford et al., 1997; Palmiter et al., 2000). Contractile proteins were added to the experimental flow cell chamber with the following series of solution incubations: 1) 20 μl of 1 μg ml^{-1} skeletal myosin or mutant HMM for 2 min.; 2) 20 μl of 0.5 mg ml^{-1} bovine serum albumin in MB for 1 min.; 3) 3 × 20 μl AB; and 4) 3 × 20 μl of AB with desired ligands, TRITC-actin, and NEM-coated beads. For the mutant HMM, two additional incubations were required to attach HMM to the flow cell surface (Trybus and Henry, 1989): an initial incubation with 20 μl of 0.1 M monoclonal antibody S2.1 for 2 min. followed by 20 μl of 0.5 mg ml^{-1} bovine serum albumin in MB for 1 min. Experiments were performed at 25°C.

By manipulating the microscope stage, a bead was captured in each of the two laser traps and the ends of a single actin filament were then attached to the beads. After pre-tensioning the filament (~4 pN), the bead-actin-bead was brought near a silica pedestal sparsely coated with myosin. The bright-field image of one of the beads was projected onto a quadrant photodiode detector and separate signals were acquired for bead movement in directions parallel and perpendicular to the actin filament's long axis. Both signals were recorded for at least ~120 s (a data record) before moving the bead-actin-bead to another pedestal within the flow cell. Data records were rejected if displacements were detected in the direction perpendicular to the filament's long axis. The remaining data records were digitized at 4 kHz after initial filtering at 2 kHz.

In vitro motility

Fluorescent images of actin filament movement over a myosin-coated surface were recorded as previously described (Warshaw et al., 1990). The solutions used in these experiments were nearly identical to those used in our laser trap experiments with the exceptions that the myosin concentration was 100 μg/ml and the final AB contained methylcellulose (Palmiter et al., 2000). Experiments were performed at 25°C. Actin filament velocities, V, were determined by analyzing video recordings of filament motility using an ExpertVision motion analysis system (Motion Analysis, Santa Rosa, CA) as previously described (Homsher et al., 1993).

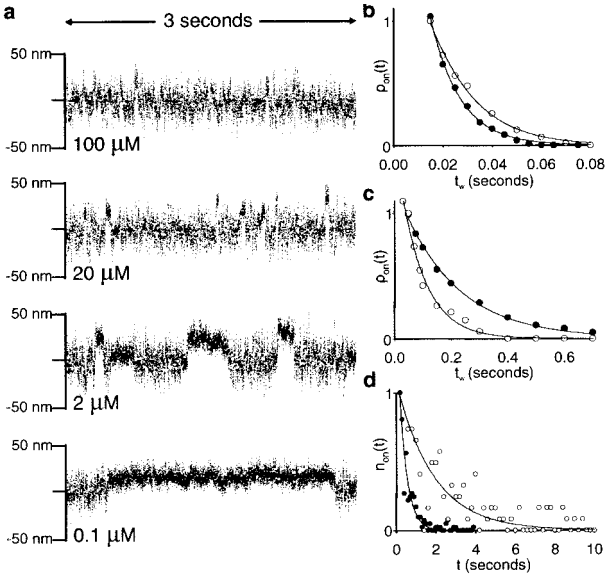

FIGURE 2 Effects of [ATP] on t_{on}. (*a*) Four characteristic data records acquired at different ATP concentrations illustrate an increase in event durations, t_{on}, with decreasing [ATP]. (*b*) Characteristic plots of MV densities, $\rho_{on}(t_w)$, versus window widths, t_w, obtained from individual data records acquired at 100 (●) and 20 μM (○) ATP fitted to Eq. 2 (*lines*). Densities at 15 ms (corresponding to $N = 107$ and 45 events for 20 and 100 μM ATP, respectively) are normalized to one. (*c*) Characteristic plots of MV densities, $\rho_{on}(t_w)$, versus window width, t_w, obtained from individual data records acquired at 1 (●) and 2 μM (○) ATP are fitted to Eq. 4 (*lines*). Densities at 50 ms (corresponding to $N = 32$ and 36 events for 1 and 2 μM ATP, respectively) are normalized to one. (*d*) Characteristic plots of $n_{on}(t)$ obtained from data records acquired at 0.5 (●, $\Delta t = 0.1$ s) and 0.1 (○, $\Delta t = 0.2$ s) μM ATP are fitted to Eq. 3. Numbers of events at 200 ms (14 and 53 for 0.1 and 0.5 μM ATP, respectively) are normalized to one. The symbols indicate the center of a bin of width Δt.

Laser trap data analysis

When myosin strongly binds to an actin filament in a laser trap, it displaces the filament and causes a reduction in the Brownian motion of the bead-actin-bead system (see Fig. 2 *a*) by adding its stiffness to the bead-actin-bead system (Molloy et al., 1995; Guilford et al., 1997). Both phenomena are used to determine when in a data trace myosin is strongly bound to actin and to calculate the duration, t_{on}, of these strong binding events.

Depending on the number of events observed in a given data trace, one of two methods was used for determining kinetic rate constants from our t_{on} data. For experimental conditions that resulted in data records containing relatively few events (i.e., <40 events in a 2-min trace), t_{on} for each event was directly measured, and for a set of data records the number of events, n_{on}, having t_{on} values between t and $t + \Delta t$ was plotted in a histogram. This distribution, $n_{on}(t)$, was then used to estimate kinetic rate constants as described below. For experimental conditions that resulted in data records containing a relatively large number of events, we used a mean-variance (MV) analysis (Patlak, 1993; Guilford et al., 1997). Briefly, this approach involves moving a time window of width t_w, point-by-point through a displacement trace and then plotting the mean and variance of each window in a two-dimensional MV histogram (see Guilford et al., 1997). These histograms are typically characterized by two regions within the MV space that contain a large number (high density) of points. One region of high variance and zero mean displacement corresponds to baseline data, whereas another region of low variance and net mean displacement corresponds to myosin displacement events (Guilford et al., 1997). Because only events with durations $\geq t_w$ appear in the event region of an MV histogram, the event density, ρ_{on}, varies with window width, t_w, reflecting the stochastic nature of event durations (i.e., the detachment kinetics). Thus, kinetic rate constants can be determined from an analysis (described below) of $\rho_{on}(t_w)$, without tallying individual events (Guilford et al., 1997).

Rate constant determination from $n_{on}(t)$ and $\rho_{on}(t_w)$ data

Two advantages of determining kinetic rate constants from single-myosin-molecule event-duration data rather than from solution kinetic or in vitro motility data are that, for each recorded event, myosin is synchronized at $t = 0$ to be in the biochemical state occupied at the onset of an event, and that we can directly determine the coupling between myosin's mechanics and kinetics without making assumptions about possible cooperative mechanical effects that may or may not exist in an ensemble preparation.

Given the scheme in Fig. 1, we can determine kinetic rate constants from an analysis of $n_{on}(t)$ and $\rho_{on}(t_w)$ distributions acquired at various ligand concentrations. According to this scheme, detachment is a two-step biochemical process and, in the absence of P_i, three rates contribute to a t_{on} distribution: the effective ADP release rate, k_{-D}, the ADP binding rate, k_D, and the second-order ATP-induced dissociation rate, k_T. Lu et al. (1998) showed that, for a two-step process, the number of events, $n_{on}(t)$, having t_{on} values between t and Δt is

$$n_{on}(t) = \frac{Ak_{-D}k_T[ATP]}{2p}\{\exp[(p+q)t] - \exp[(q-p)t]\}, \quad (1)$$

where

$$p = \sqrt{.25(k_{-D} + k_D[ADP] + k_T[ATP])^2 - k_{-D}k_T[ATP]},$$

$$q = -\tfrac{1}{2}(k_{-D} + k_D[ADP] + k_T[ATP]),$$

and A is the product of Δt and the number of events in the data set, N. Values for k_D, k_{-D}, and k_T can thus be determined by fitting a distribution, $n_{on}(t)$, of individually measured t_{on} values to Eq. 1. These rate constants can also be determined by fitting MV window densities, $\rho_{on}(t_w)$, to the equation

$$\rho_{on}(t_w) = \frac{Bk_{-D}k_T[ATP]}{2p} \times \left\{\frac{1}{(p+q)^2}\exp[(p+q)t_w] - \frac{1}{(q-p)^2}\exp[(q-p)t_w]\right\}, \quad (2)$$

where B is the product of N and the sampling frequency (Patlak, 1993), and p and q are defined as above for Eq. 1.

When detachment is limited by a single biochemical step, Eq. 1 reduces to

$$n_{on}(t) = Ak_{rls}\exp(-k_{rls}t), \quad (3)$$

where k_{rls} is the rate of the limiting step. In the absence of ADP and at sufficiently low ATP concentrations ($[ATP]k_T \ll k_{-D}$), detachment is limited by ATP binding, and k_{rls} equals $k_T[ATP]$. At sufficiently high ATP concen-

trations ([ATP]$k_T \gg k_{-D}$), detachment is limited by ADP release, and k_{rls} equals k_{-D}. The analogous equation for data gathered through MV analysis is

$$\rho_{on}(t_w) = (B/k_{rls})\exp(-k_{rls}t_w). \quad (4)$$

Event lifetime determination

The duration of a given event is t_{on}, and the average duration of many events is the event lifetime, τ_{on}, which can be calculated using one of two methods. One approach is to simply average individually measured t_{on} values. However, this approach is valid only if an event population does not contain a significant number of events with durations shorter than the laser trap dead time (<2 ms). The second approach is to calculate τ_{on} from the rate constants determined above (i.e. k_{-D}, k_D, and k_T). Solving

$$\tau_{on} = \frac{1}{A}\int_0^\infty t n_{on}(t)\, dt,$$

substituting $n_{on}(t)$ from Eq. 1, we obtain an expression for τ_{on} as a function of k_{-D}, k_D, and k_T

$$\tau_{on} = \frac{k_{-D}k_T[ATP]}{2p}\left\{\frac{1}{(p+q)^2} - \frac{1}{(q-p)^2}\right\} \quad (5)$$

where p and q are defined as above for Eq. 1.

RESULTS

The effects of [ATP] on single molecule and ensemble kinetics

The lifetime of the strongly bound state in the absence of ADP and P_i is related to k_{-D} and k_T (Palmiter et al., 1999) as

$$\tau_{on} = \frac{1}{k_{off}} = \frac{1}{k_{-D}} + \frac{1}{k_T[ATP]} = \frac{1}{k_{-D}} + \frac{K_{M(on)}}{k_{-D}[ATP]}, \quad (6)$$

where $K_{M(on)} = k_{-D}/k_T$ is the ATP concentration at which τ_{on} is twice its minimum value (i.e., $1/k_{-D}$ at saturating ATP). This relationship is obtained by setting [ADP] = 0 in Eq. 5. Eq. 6 predicts that τ_{on} should increase when [ATP] is decreased, reaching an ATP-limited value of $\tau_{on} \sim 1/k_T[ATP] \sim 1/k_{rls}$ at sufficiently low [ATP]. As predicted, Fig. 2 qualitatively shows that τ_{on} for skeletal muscle myosin increased when we decreased [ATP] from 100 to 0.1 μM, and at 2 μM ATP τ_{on} appeared to be at least an order of magnitude longer than τ_{on} at 100 μM ATP (i.e., $1/k_T[ATP] \gg 1/k_{-D}$ thus τ_{on} is limited by $k_T[ATP]$). Therefore, for each experiment performed at [ATP] $\leq$ 2 μM, we obtained a value for k_{rls} either by fitting MV densities, $\rho_{on}(t_w)$, to Eq. 4 (1 and 2 μM ATP; Fig. 2 *c*) or by fitting distributions of individually measured t_{on} values, $n_{on}(t)$, to the corresponding relationship in Eq. 3 (0.1 and 0.5 μM ATP; Fig. 2 *d*). In Fig. 3, we plotted the average k_{rls} estimated at each [ATP] with the slope of the regression giving a value for k_T of 7.6 $\times$ 10^6 M^{-1} s^{-1} (see Fig. 3, legend).

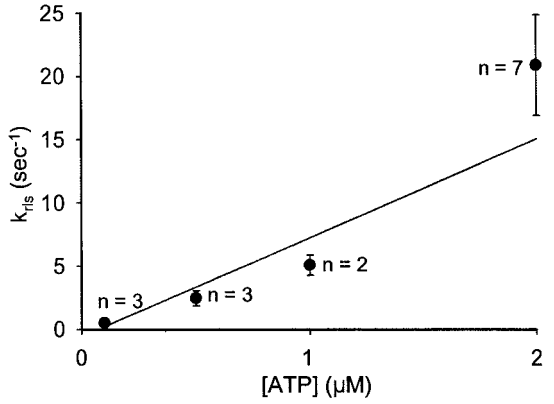

FIGURE 3 k_{rls} versus [ATP]. Values for k_{rls} determined from $\rho_{on}(t_w)$ and $n_{on}(t)$ data acquired at [ATP] $\leq$ 2 μM are plotted for different ATP concentrations. Each point is the average value obtained from n data records (each containing >40 events) with error bars representing the SEM. The slope of a regression weighted by 1/SEM (*line*) gives a value for k_T of 7.6 ($\pm$ 1.3 SEM) $\times$ 10^6 M^{-1} s^{-1}. A 95% confidence interval gives values for k_T ranging from 5 to 12.5 $\times$ 10^6 M^{-1} s^{-1}. It is possible that, at 2 μM ATP, the t_{on} distribution might not be fully limited by k_T[ATP], which might explain why this point appears not to be described by the linear regression. A regression that excludes this point gave a value for k_T of 5 $\times$ 10^6 M^{-1} s^{-1}.

At 10 μM ATP, τ_{on} was not an order of magnitude longer than τ_{on} at 100 μM, and thus was not limited by k_T[ATP]. Therefore, to account for the effects of both ADP release and ATP binding, we fitted MV densities, $\rho_{on}(t_w)$, acquired at [ATP] $\geq$ 10 μM (10, 20, and 100 μM) to Eq. 2 (for examples, see Fig. 2 *b*). Setting k_T equal to the value determined above, the fits gave an average value for k_{-D} of 100 s^{-1} (Table 1). Based on our estimates for k_{-D} and k_T, we calculate a value for $K_{M(on)} = k_{-D}/k_T$ of 13 $\pm$ 3 μM.

To compare the detachment kinetics (k_{-D} and k_T) of a single skeletal muscle myosin molecule with the motion-generating biochemistry of an ensemble of myosin molecules, we measured actin filament velocities, V, in a motility assay over [ATP] ranging from 0.01 to 1.0 mM. The rela-

TABLE 1 Rate constants obtained from single molecule t_{on} data

k_T (10^6 M^{-1} s^{-1})	k_{-D} (s^{-1})	$K_M = k_{-D}/k_T$ (μM)	k_D (10^5 M^{-1} s^{-1})	k_{Pi} (10^3 M^{-1} s^{-1})
7.6 $\pm$ 1.3*	100 $\pm$ 6†	13 $\pm$ 3‡	2.7 $\pm$ 0.3§	1.1 $\pm$ 0.4¶

*Value $\pm$ SEM obtained from slope of regression in Fig. 3.
†Value $\pm$ SEM obtained from n = 15 data records, each containing >40 events.
‡Value $\pm$ propagated error calculated from $K_M = k_{-D}/k_T$.
§Value $\pm$ SEM obtained from n = 15 data records, each containing >40 events.
¶Value $\pm$ SEM obtained from least squares fit in Fig. 7 *b*.

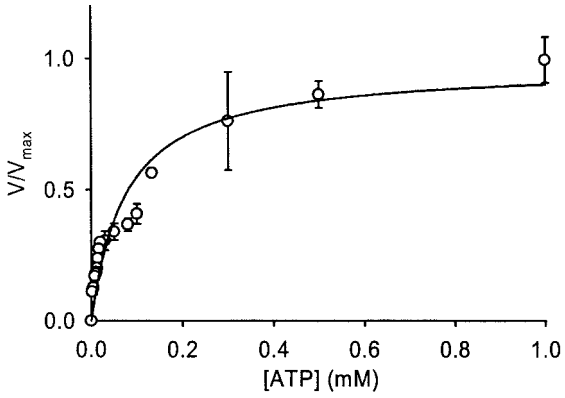

FIGURE 4 V/V_{max} versus [ATP]. Actin velocities measured in a motility assay are plotted for different ATP concentrations and are fitted to Eq. 7 (*line*), giving a value for K_M of 76 ± 17 μM (SEM). V_{max} is 2.6 μm s^{-1}. Each data point represents the average velocity from four different experiments, and the error bars represent the SEM. All four experiments showed a similar [ATP] dependence.

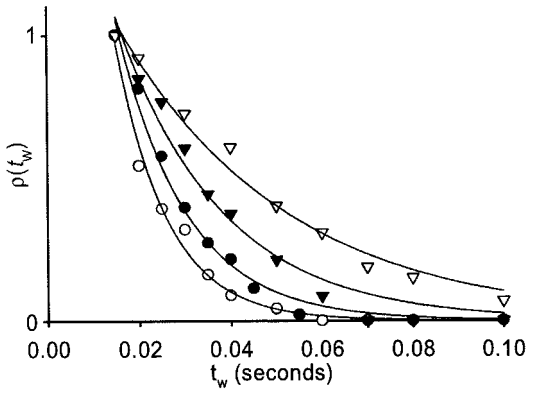

FIGURE 5 Effects of [ADP] on t_{on}. Characteristic plots of MV densities, $\rho_{on}(t_w)$, versus window width, t_w, obtained from data records acquired at 100 μM ATP and 0 (○), 1 (●), 2.5 (▼), and 5 (▽) mM ADP are fit to Eq. 2 (*lines*). Plots are normalized to the MV density at 20 ms.

tionship between V and [ATP] is often assumed to follow a Michaelis–Menten equation,

$$V = \frac{V_{max}[ATP]}{[ATP] + K_{M(vel)}}, \quad (7)$$

where $K_{M(vel)}$ is the ATP concentration at which the velocity is half its maximum value, V_{max}. We fitted our motility data to Eq. 7, with the fit giving a value for $K_{M(vel)}$ of 76 μM (Fig. 4). This value is comparable to previously reported values for monomeric skeletal muscle myosin in a motility assay (Homsher et al., 1993), but it is approximately five-fold greater than the value for $K_{M(on)}$ estimated from our single molecule data above. This five-fold difference is surprising because actin velocities are often assumed to be limited by τ_{on}, in which case $K_{M(vel)}$ should be equal to $K_{M(on)}$ (see Discussion and Appendix).

The effects of [ADP] on single molecule and ensemble kinetics

We determined the effective ADP binding rate, k_D, from MV distributions, $\rho_{on}(t_w)$, acquired at 100 μM ATP and various ADP concentrations (0–5 mM; Fig. 5). We chose 100 μM ATP rather than 1 mM ATP because event durations at 1 mM ATP are only marginally within our temporal resolution (τ_{on} was estimated by Finer et al. (1994) to be <5 ms). We observed that τ_{on} increased when we added ADP. We fitted MV distributions, $\rho_{on}(t_w)$, acquired at different [ADP] to Eq. 2 (Fig. 5, *solid lines*), setting $k_T = 7.6 \times 10^6$ M^{-1} s^{-1} and $k_{-D} = 100$ s^{-1} as determined above. The fits gave an average value for k_D of 2.7×10^5 M^{-1} s^{-1} (Table 1).

To determine the effects of [ADP] on actin filament velocities, V, we performed motility experiments under conditions (100 μM ATP and 0–5 mM ADP) similar to those used above in our single-molecule experiments. The velocities acquired at different ADP concentrations are plotted in Fig. 6, and show that V slowed when we added ADP. We fitted these data to a variation of Eq. 7 (see Fig. 6, legend), and the fit gave a value for an ADP inhibition constant, $K_{I(vel)}$, of 222 μM.

The effects of P_i on single molecule and ensemble kinetics

According to the scheme in Fig. 1, myosin can detach from actin through one of two pathways: ATP binding to the A·M state or P_i binding to the A·M·D state. To test this hypothesis, we acquired single-molecule displacement data from skeletal muscle myosin at 0.1 μM ATP both in the presence

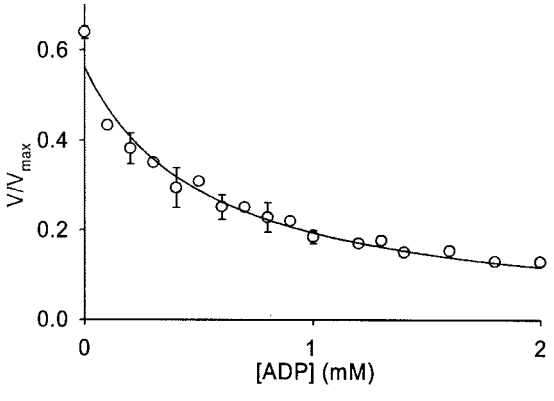

FIGURE 6 V/V_{max} versus [ADP]. Actin velocities measured in a motility assay are plotted for different ADP concentrations and fitted to $V/V_{max} = [ATP]/\{[ATP] + K_{M(vel)}(1 + [ADP]/K_{I(vel)})\}$. This relationship is obtained by substituting $K_{M(vel)}$ for $K_{M(vel)}(1 + [ADP]/K_{I(vel)})$ in Eq. 7, where $K_{I(vel)}$ is an inhibition constant. The fit gave a value for $K_{I(vel)}$ of 222 μM, when $K_{M(vel)}$ was set to the value of 76 μM obtained from our ATP-dependent motility data. V_{max} is 2.6 μm s^{-1}. Each data point represents the average velocity from three different experiments, and the error bars represent the SEM.

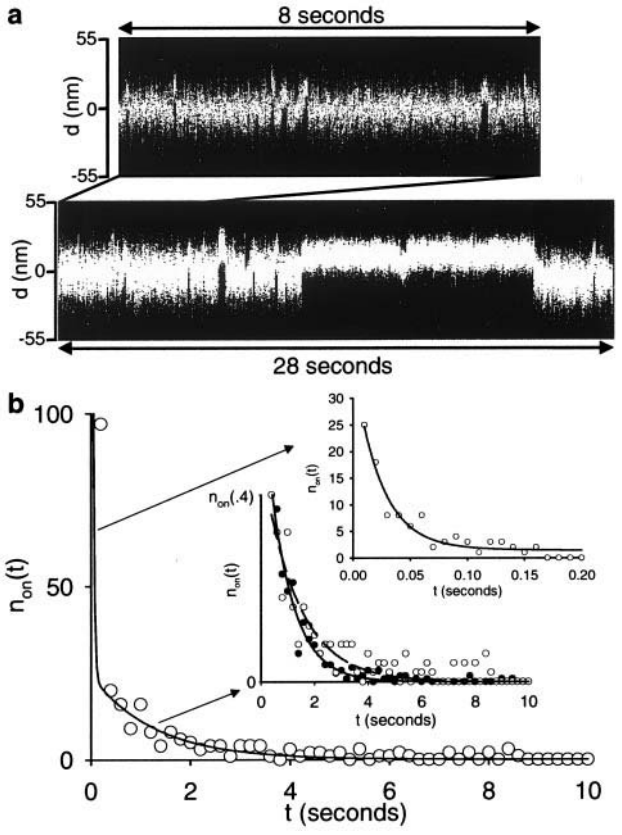

FIGURE 7 Effects of P_i on t_{on}. (*a*) A characteristic data trace acquired at 0.1 μM ATP and 40 mM P_i contains some long events (*lower trace*) and an inordinately large number of short events (*expanded scale*, *upper trace*). (*b*) Event densities, $n_{on}(t)$, acquired at 0.1 μM ATP and 40 mM P_i indicate a short event population that is contained within the first Δt = 200-ms bin (*point*), with the remainder of the points belonging to a significantly longer event population. (*Lower inset*) The long event population is replotted and fit to Eq. 3 (*dashed line*), giving a value for k_T of 7.8 $\times$ 10^6 M^{-1} s^{-1} that is similar to the value of 11.3 $\times$ 10^6 M^{-1} s^{-1} obtained from a fit (*solid line*) to the data (*solid circles*) acquired in the absence of added P_i. Plots are normalized to the number of events at 400 ms. *Upper inset*: The first 200-ms bin (containing the short event population) is expanded into smaller 10-ms bins (*open circles*) and is fit to Eq. 8, setting k_{-D} = 100 s^{-1} and k_T = 7.8 $\times$ 10^6 M^{-1} s^{-1}. The fit gives a value for k_{Pi} of 1.1 $\times$ 10^3 M^{-1} s^{-1}. The curve (*solid line*) in Fig. 7 *b* (*large graph*) is a plot of Eq. 8, with k_{-D} = 100 s^{-1}, k_{Pi} = 1.1 $\times$ 10^3 M^{-1} s^{-1}, and k_T = 7.8 $\times$ 10^6 M^{-1} s^{-1}.

(Fig. 7 *a*) and absence of 40 mM P_i. We chose these conditions in an attempt to clearly separate the lifetimes of the two detachment processes. For P_i to induce myosin detachment, P_i must bind to myosin prior to ADP release. Thus, if we are to observe a significant population of P_i-induced detachments, the concentration of P_i must be sufficiently high so that the probability of P_i binding is comparable to the probability of ADP release. To distinguish a P_i-dependent t_{on} population from an ATP-dependent t_{on} population, we chose a low ATP concentration of 0.1 μM ATP. We estimate the ATP-dependent lifetime of the A·M state to be ~1300 ms at 0.1 μM ATP, which is significantly longer than the ~10 ms lifetime of the A·M·D state determined above.

In Fig. 7 *a*, a portion of a data trace acquired at 0.1 μM ATP and 40 mM P_i contains some long events along with an inordinate number of short events. In Fig. 7 *b*, we plotted the $n_{on}(t)$ distribution from these experiments, and the data clearly indicate the presence of two event populations. One population has long event durations characteristic of those expected at 0.1 μM ATP and the other event population, only observed in the presence of P_i, has short event durations. Thus it appears that these long- and short-event populations correspond to the ATP- and P_i-induced detachment processes, respectively. These two independent processes should result in two independent $n_{on}(t)$ distributions. The short-event population appears to be completely contained within the first 200-ms bin (Fig. 7 *b*), and thus the remainder of the data should be described by the $n_{on}(t)$ distribution predicted for the long (ATP-induced) population alone, which, at low [ATP], is $Ak_T[ATP]\exp(-k_T[ATP]t)$ (Eq. 3). In the lower inset of Fig. 7 *b*, we fitted the long-event data (*open circles*) to this equation, setting k_{-D} = 100 s^{-1}. The fit (*dashed line*) gave a value for k_T of 7.8 ($\pm$ 0.7) $\times$ 10^6 M^{-1} s^{-1}, which is comparable to the value for k_T of 11.3 ($\pm$ 0.6) $\times$ 10^6 M^{-1} s^{-1} obtained when we fitted (*solid line*) 0.1 μM ATP data (*closed circles*) acquired in the absence of P_i to the same equation. Analogous to $n_{on}(t)$ for the ATP-induced population, the $n_{on}(t)$ distribution for the P_i-induced population is $Ak_{Pi}[P_i]\exp(-k_{Pi}[P_i]t)$. Because the fraction of the total number of events in the $n_{on}(t)$ distribution attributable to the ATP-dependent pathway is $k_{-D}/(k_{-D} + k_{Pi}[P_i])$ and the fraction attributable to the P_i-dependent pathway is $k_{Pi}/(k_{-D} + k_{Pi}[P_i])$, the overall $n_{on}(t)$ distribution predicted for these experiments is

$$n_{on}(t) = A\left\{\frac{k_{-D}}{k_{-D} + k_{Pi}[P_i]}\,k_T[ATP]\exp(-k_T[ATP]t) + \frac{k_{Pi}[P_i]}{k_{-D} + k_{Pi}[P_i]}\,k_{Pi}[P_i]\exp(-k_{Pi}[P_i]t)\right\}. \quad (8)$$

In the upper inset of Fig. 7 *b*, we expanded the first 200-ms bin (which contains the short-event population) into smaller 10-ms bins, and we fitted these data to Eq. 8 after setting k_{-D} = 100 s^{-1} and k_T = 7.8 $\times$ 10^6 M^{-1} s^{-1}. The fit gave a value for k_{Pi} of 1.1 ($\pm$ 0.4) $\times$ 10^3 M^{-1} s^{-1}. In the discussion, we use these results to assess the timing of myosin's mechanical step relative to P_i release.

The effects of a myosin mutation that inhibits P_i release

To investigate further the timing of the mechanical step relative to P_i release, we used an expressed smooth muscle HMM mutation that has been shown to limit actin's ability to accelerate P_i release (k_{-Pi} in Fig. 1 is reduced to less than

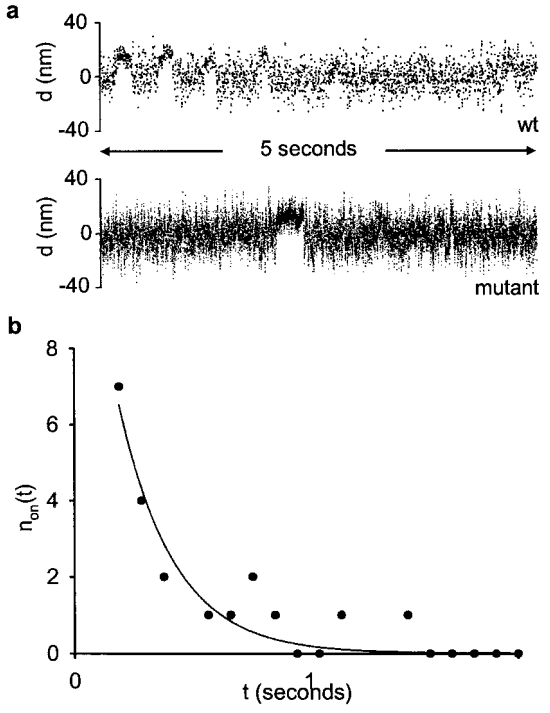

FIGURE 8 Effects of a P_i release rate myosin mutation on τ_{on}. (*a*) Characteristic data records are shown for both wild-type smooth muscle myosin (*upper trace*; data from Lauzon et al., 1998) and mutant smooth muscle myosin (*lower trace*; see text for mutant details). (*b*) The $n_{on}(t)$ distribution obtained from mutant data records.

0.2 s^{-1}) without significantly altering the kinetics of other steps in the biochemical cycle (Joel et al., 2001). A similar mutation in skeletal muscle myosin would have provided a more direct comparison with the above data but was unavailable. Nevertheless, because the same mechanochemical scheme (Fig. 1) is thought to apply to all muscle myosin types, the relationship between myosin's mechanical step and P_i release measured in smooth muscle HMM should be the same as that for skeletal muscle myosin. If myosin's mechanical step precedes P_i release, then we would expect this mutation would significantly increase the event lifetime, whereas, if the mechanical step occurs with or after P_i release, then we would expect this mutation would reduce the event frequency without affecting the event lifetime.

We acquired displacement data from the mutant at 10 μM ATP so that we could compare these data with our previous displacement data acquired from wild-type smooth muscle HMM (Lauzon et al., 1998). We observed a displacement event frequency of <0.1 s^{-1}, which is considerably less than the frequency of ~ 2 s^{-1} observed for the wild type. This may explain why the mutant does not support actin filament movement in an in vitro motility assay (Joel et al., 2001). From the events that we did observe (Fig. 8), we measured an average step size of ~ 8 nm, comparable to that previously reported for the wild-type control (Lauzon et al., 1998). Moreover, we calculated an event lifetime of $\tau_{on} = 198 \pm 76$ ms that is also comparable to the lifetime of $\tau_{on} = 158$ ms previously reported for the wild-type myosin at 10 μM ATP (Lauzon et al., 1998). These results, showing that the mutation decreases event frequency without significantly altering event lifetimes, indicate that the mechanical step occurs with or after P_i release.

DISCUSSION

The kinetics of the actomyosin ATPase reaction have been characterized extensively both in solution and in muscle fiber preparations (for reviews see Goldman 1987, and Sellers 1999), and a minimal scheme is presented in Fig. 1. In the present study, we used the laser trap assay to characterize the effects of substrate (ATP) and product (ADP, P_i) concentrations on event durations, t_{on}, of single myosin molecules, and the observed effects were accounted for by this scheme. Using a kinetic analysis based on this scheme, we determined rate constants (summarized in Table 1) from t_{on} distributions acquired under nearly unloaded conditions, low ionic strength, a temperature of 25°C, and a pH of 7.4. In parallel experiments, we used an in vitro motility assay to characterize how changes in substrate and product concentrations affected the actin velocity generated by an ensemble of myosin molecules. Here we compare our single molecule data (acquired under nearly unloaded conditions) with previous solution kinetic studies (acquired under fully unloaded conditions), and discuss apparent discrepancies, focusing on possible differences between the two assays. Moreover, we compare our single-molecule data with our ensemble velocity data (presumably limited by the load of actin-attached myosin), using a model in which myosin's mechanical step is partitioned between moving an actin filament and generating force.

Kinetics of the actomyosin ATPase cycle

By varying [ATP] from 0.1 to 100 μM, we determined values for the second-order ATP-induced dissociation rate ($k_T = 7.6 \times 10^6$ M^{-1} s^{-1}) and the effective ADP release rate ($k_{-D} = 100$ s^{-1}). The value we obtained for k_T is similar to the value of 5.5×10^6 M^{-1} s^{-1}, whereas the value for k_{-D} is lower than the value of >300 s^{-1} estimated from solution studies of fast chicken skeletal muscle subfragment-1 (Marston and Taylor, 1980). One possible explanation for this three-fold difference between k_{-D} values is that the slight positive strain that exists in the laser trap (~ 0.4 pN) may decrease the ADP release rate below that of unloaded myosin in solution. This explanation is supported by evidence suggesting that k_{-D} is highly strain sensitive. For example, in skinned psoas fiber studies k_{-D} was estimated to be 13.5 s^{-1} for positively strained myosin but increased to as high as 400 s^{-1} when the myosin was negatively strained (Dantzig et al., 1991). Moreover if, as

assumed in the original Huxley (1957) two-state crossbridge model, the rate of crossbridge detachment (g) is strain dependent, then, considering that detachment is limited by ADP release under physiological conditions (Siemankowski et al., 1985; Weiss et al., 2001), ADP release would be the strain-dependent step in the detachment process.

Another possible explanation for the three-fold difference between the value for k_{-D} estimated in the present study and that measured in solution studies is that k_{-D} in our analysis may not be the ADP release rate measured in solution studies. In our analysis, k_{-D} is the effective rate at which myosin releases ADP, starting from the state occupied at the onset of strong binding, whereas, in solution studies, k_{-D} is the rate at which myosin releases ADP starting from the state occupied following the addition of ADP to the A·M state. Thus a relatively slow myosin isomerization that follows strong actin binding and precedes ADP release (A·M*·D → A·M·D; Sleep and Hutton, 1980) would account for the relatively low value for k_{-D} estimated from the laser trap assay.

From the laser trap experiments in which we varied [ADP], we determined a second-order ADP-binding rate, k_D, of $2.7 \times 10^5\ M^{-1}\ s^{-1}$. This value is similar to the value of 1.5 to $3.8 \times 10^5\ M^{-1}\ s^{-1}$ reported for skinned psoas fibers (Dantzig et al., 1991) but is an order of magnitude less than the ADP binding rate obtained from solution studies (Geeves, 1989). One possible explanation for why values for both k_{-D} and k_D determined in the laser trap are significantly less than the ADP binding and release rates measured in solution studies is that structural constraints in the laser trap assay may restrict the thermal fluctuations of the actomyosin system, effectively increasing the activation energy barrier for both ADP binding and release rates. Another possible explanation is that, as argued above for k_{-D}, a significantly populated A·M*·D state exists, which is not included in our kinetic analysis, resulting in an underestimate of k_D.

Kinetics of the mechanical step

The largest free energy drop within the actomyosin ATPase cycle is associated with P_i release (White and Taylor, 1976). Therefore, the motion-generating step of the cycle has been linked to this biochemical transition. However, the timing of the mechanical step relative to the release of P_i has yet to be determined. To address this question, we took advantage of a myosin mutation that significantly reduces the actin-activated P_i release rate. We showed that the mutation had little effect on the event lifetime, implying that the mechanical step could not occur prior to the biochemical transition affected by the mutation (i.e., P_i release) and thus must occur after or concomitant with P_i release.

To further test the hypothesis that the mechanical step is closely associated with P_i release, we analyzed t_{on} distributions for skeletal muscle myosin acquired at 0.1 μM ATP both in the presence and absence of added P_i. Our data imply that P_i can induce myosin detachment from actin via a pathway distinct from the ATP-induced actin dissociation pathway (Fig. 1). Our data do not rule out the existence of a strong-binding ternary complex (A·M·D·P_i), but they do place limits on its lifetime and temporal relationship to the mechanical step. We consider the following scheme:

$$\underset{\text{weak}}{MDP_i} \underset{k_{-A}}{\overset{k_{+A}}{\rightleftharpoons}} \underset{\text{strong?}}{AMDP_i} \underset{k_{+Pi}}{\overset{k_{-Pi}}{\rightleftharpoons}} \underset{\text{strong}}{AMD}$$

SCHEME 1

If the A·M·D·P_i state in Scheme 1 is a strong binding state that precedes a mechanical step, the lifetime of this state must be shorter than the time resolution of our laser trap assay (<2 ms). This follows from the fact that we do not detect a change in variance (the signature of strong binding) that precedes a mechanical step. A similar conclusion was reached based on single-myosin molecule fluorescence polarization measurements (Warshaw et al., 1998) and rapid freezing EM images (Walker et al., 1999).

If the A·M·D·P_i state in Scheme 1 is a strong binding state that follows a mechanical step, as concluded from several different muscle fiber mechanics studies (Kawai and Halvorson, 1991; Dantzig et al., 1992; Walker et al., 1992), the lifetime of this state must also be extremely short. This follows from the fact that we do not observe an event population with a short lifetime in the absence of P_i, and so, either the lifetime of this state must be shorter than the time resolution of our assay (i.e., in Scheme 1, $1/k_{-A} < 2$ ms), or the probability of actin dissociation from this state is low relative to P_i release (i.e., in Scheme 1, $k_{-Pi} \gg k_{-A}$). For the latter case, our data show that k_{-A} is at least 44 s^{-1} ($k_{-A} > 1.1 \times 10^3\ M^{-1}\ sec^{-1} \times 40$ mM), and so k_{-Pi} in Scheme 1 must have a value greater than 400 s^{-1} to explain the absence (<10%) of a short t_{on} population at low [ATP] and no added P_i. Thus, if a strongly bound A·M·D·P_i state follows the mechanical step, it must have a relatively short lifetime (<3 ms). Of those muscle mechanics studies that imply the existence of this state, most imply that it is short-lived (Fortune et al., 1991; Ranatunga, 1999). In general, our single-molecule data suggest that strong-binding A·M·D·P_i states, whether they precede or follow the mechanical step, are not metastable states; i.e., they are extremely short lived (<3 ms). Within the current time resolution of our detection system, it appears that myosin's mechanical step is closely associated with both P_i release and strong actin binding (Fig. 1).

Comparison of single molecule and ensemble data

We have shown that a laser trap assay can be used to directly correlate the mechanics and kinetics of the actomy-

osin ATPase cycle. In the past, the in vitro motility assay was thought to be capable of serving a similar purpose. Two equations have typically been used for extrapolating kinetic constants from the ATP-dependence of actin velocities, V, measured in a motility assay; they are $V = \bar{d}/\tau_{on}$ and the Michaelis–Menten equation, $V = V_{max}[ATP]/([ATP] + K_{M(vel)})$. However, neither expression accurately describes our velocity data acquired over all ATP concentrations. First, we observed that $K_{M(vel)}$ differed from $K_{M(on)}$. Second, the relationship between actin velocities and ATP concentration was not accurately described by a Michaelis–Menten equation (see least squares fit in Fig. 4). Implicit in the two equations above is the assumption that the load of actin-attached myosin molecules in a motility assay fully limits actin movement without affecting actin-myosin detachment kinetics measured in a single molecule laser trap assay. It appears that a better understanding of the relationship between actin–myosin ATPase kinetics, myosin's mechanical step, load, and actin velocity is needed.

In the Appendix, we develop a simple model of myosin-based actin movement. Briefly, we assume that, when a mechanical step (defined here to include the mechanism by which actin is moved in an unloaded laser trap) occurs against a resistive load, it is partitioned between moving an actin filament and stretching internal compliant elements in the actomyosin system. In one extreme limit of the model (Appendix, Case 2), actin-attached myosin heads in an ensemble impose a high-resistive load against which a mechanical step can only generate force (i.e., it stretches compliant elements). This is the classic detachment-limited model of actin motility, and indeed for the case in which a single biochemical step limits detachment, we derived the widely used relationship $V = \bar{d}/\tau_{on}$. The general expression we derived for the ATP-dependence of V (Eq. A2) is non-Michaelian, but its deviation from a Michaelis–Menten (hyperbolic) relationship is relatively subtle and still does not account for the more dramatic departure from a hyperbolic relationship exhibited by our data at high [ATP] (see Fig. 9 *a*). Nevertheless, we use this model as a starting point for a quantitative comparison of our single molecule and ensemble data as follows.

In Fig. 9 *a*, we replotted our velocity data as $\bar{d}/V$ (which, according to a detachment-limited model, should roughly equal τ_{on}) versus 1/[ATP], and, on the same graph, we plotted our single molecule τ_{on} data versus 1/[ATP]. Figure 9 *a* shows that, at [ATP] $<$ 100 μM, our motility data roughly follow our τ_{on} data (i.e., $V = \bar{d}/\tau_{on}$) and exhibit Michaelis–Menten behavior (i.e., a linear relationship in a double reciprocal plot) as predicted by a detachment-limited model. Even the apparent slight downward curvature in the low [ATP] velocity data is predicted by our detachment-limited model (Eq. A2) as a transition from velocities limited by ATP binding (at low [ATP]) to velocities limited by ADP release (at high [ATP]). A least squares fit of these low [ATP] motility data to Eq. A2 (Fig. 9 *a*, *red line*) gave

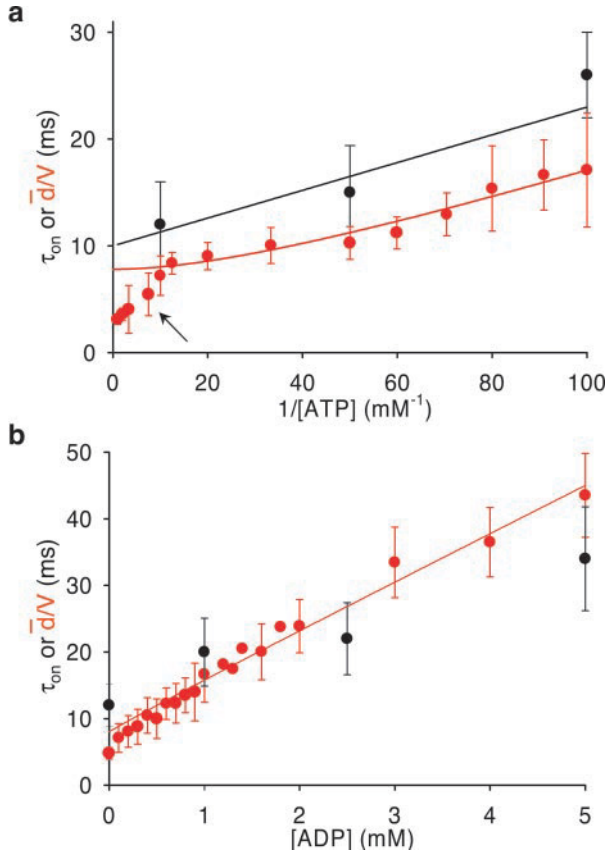

FIGURE 9 Effects of [ATP] and [ADP] on τ_{on} and V. (*a*) From single molecule data acquired at [ATP] $\geq$ 10 μM and no added ADP or P_i, τ_{on} values were calculated using Eq. 6, with $k_T = 7.6 \times 10^6$ M^{-1} s^{-1} and k_{-D} set to the values obtained at each [ATP]. These τ_{on} values (*black circles*), along with values for $\bar{d}/V$ (*red circles*, $\bar{d}$ = 8 nm), are plotted versus 1/[ATP]. The black line is Eq. 6, with $k_T = 7.6 \times 10^6$ M^{-1} s^{-1} and k_{-D} = 100 s^{-1}. The velocity data acquired at [ATP] $<$ 100 μM is fit to Eq. 10 (*red line*), with the fit giving values for k_{-D}, k_T, and $K_M = k_{-D}/k_T$ of 128 s^{-1}, 7.0 $\times$ 10^6 M^{-1} s^{-1}, and 18 μM respectively. (*b*) For single-molecule data acquired at 100 μM ATP and various [ADP], τ_{on} values were calculated from Eq. 5, setting k_{-D} = 100 s^{-1} and $k_T = 7.6 \times 10^6$ M^{-1} s^{-1}. These values (*black circles*), along with values for $\bar{d}$/V (*red circles*, $\bar{d}$ = 8 nm), are plotted versus [ADP]. The velocity data are fit to Eq. 9, setting k_{-D} = 128 s^{-1} and $k_T = 7 \times 10^6$ M^{-1} s^{-1}. The fit gave a value for k_D of 5.1 $\times$ 10^5 M^{-1} s^{-1}.

values for k_{-D}, k_T, and $K_M = k_{-D}/k_T$ of 128 $\pm$ 9 s^{-1}, 7.0 ($\pm$ 0.8) $\times$ 10^6 M^{-1} s^{-1}, and 18 $\pm$ 3 μM respectively. These values are in excellent agreement with those obtained from our single-molecule data for k_{-D}, k_T, and K_M of 100 s^{-1}, 7.6 $\times$ 10^6 M^{-1} s^{-1}, and 13 μM, respectively.

We also used this model to compare the ADP-dependence of our single-molecule and ensemble data by plotting both $\bar{d}/V$ for motility data and our single-molecule τ_{on} data versus [ADP] (Fig. 9 *b*). Once again, our motility data appear to follow our τ_{on} data as $V \sim \bar{d}/\tau_{on}$. A fit of our motility data to Eq. A1 provides estimates for k_D of 5.1 $\times$ 10^5 M^{-1} s^{-1} (see Fig. 9 *b*, legend), which is comparable to the value of $k_D = 2.7 \times 10^5$ M^{-1} s^{-1} estimated from our

single-molecule experiments. Thus it appears that the detachment-limited model of actin velocities (Appendix, Case 2) accurately describes our velocity data acquired at [ATP] $\leq$ 100 μM both in the absence and presence of ADP.

However at [ATP] $>$ 100 μM (Fig. 9 *a*, *arrow*) our motility data deviate both from our τ_{on} data (i.e., $V \neq \bar{d}/\tau_{on}$) and from a Michaelis–Menten [ATP] dependence. When we fitted our velocity data acquired at [ATP] $>$ 100 μM to Eq. 7, we obtained a value for $K_{M(vel)}$ of 174 μM. This value is similar to values for K_M of 150–200 μM obtained from in vitro motility (Homsher et al., 1993) and muscle fiber studies (Cooke and Bialek, 1979) but is roughly an order of magnitude greater than the values for $K_{M(on)}$ and $K_{M(vel)}$ obtained from velocity data acquired at [ATP] $<$ 100 μM. Similarly, from the velocity data acquired at [ATP] $>$ 100 μM, we estimated a value for k_{-D} ($= V_{max}/\bar{d}$) of 313 s^{-1}, which is significantly greater than the value of 100 s^{-1} obtained from our single-molecule τ_{on} data. These apparent discrepancies between kinetic constants determined from V and τ_{on} data are not limited to chicken skeletal myosin. For many different myosin types, the values for k_{-D} that we estimate from actin velocities (by assuming $V = \bar{d}/\tau_{on}$) are consistently more than two-fold greater than the values for k_{-D} that we estimate from τ_{on} data (Tyska and Warshaw, 2002). What we have shown in this paper is that this apparent discrepancy has an [ATP] dependence. Our V data depart both from the relationship $V = \bar{d}/\tau_{on}$ and from a Michaelis–Menten relationship only when [ATP] is increased above 100 μM. Because the mean step size, $\bar{d}$, does not depend on [ATP] (Lauzon et al., 1998; Palmiter et al., 1999), these results indicate that the kinetics underlying V begin to change around 100 μM ATP. Thus it appears that at least one of the assumptions of our detachment-limited model (Appendix, Case 2) does not apply to our motility data acquired at [ATP] $>$ 100 μM.

Two critical assumptions of our detachment-limited model are that attached myosin heads fully prevent mechanical steps from being realized as actin movement and that detachment rates are independent of strain. Because the fraction of attached heads resisting actin movement decreases with increasing [ATP], it might be that, at [ATP] $>$ 100 μM, the fraction of attached heads is no longer sufficient to fully prevent mechanical steps from contributing to actin movement, in which case V becomes influenced by attachment kinetics (see Appendix, Case 3). An alternate explanation is that, at high [ATP], actin-attached myosin will be predominantly in the A·M·D state. Assuming a strain-dependent ADP release rate, the more negatively strained the myosin becomes at high actin filament velocities, the more rapidly ADP will be released.

Regardless of the mechanism, the basic observation that V departs, at high [ATP], from both Michaelis–Menten kinetics and our single-molecule d/τ_{on} data has significant implications for the mechanochemistry of actin movement. Actin velocities will only follow a Michaelis–Menten relationship if a single kinetic step limits velocity and if the rate constant for that step is unchanging. If varying [ATP] indirectly modulates interactions among myosin heads in the motility assay, changing the biochemical step that limits V and/or altering the rate of the limiting step, then motility data will deviate from Michaelis–Menten behavior. When we attempted to fit our velocity data to a Michaelis–Menten equation over the entire range of [ATP], we obtained a value for K_M of 75 μM (see Results). Upon further analysis, we believe that this value for K_M describes a shift from a detachment- to attachment-limited velocity or a variable ADP release rate, and that the K_M of 18 μM determined above from low [ATP] data more accurately reflects Michaelis–Menten detachment kinetics.

CONCLUSIONS

Laser traps provide a direct assay of actomyosin detachment kinetics at the level of a single myosin motor. Using this assay, we have estimated values for k_{-D}, k_T, k_D, and k_{Pi}; characterized the mechanical properties of individual biochemical states; and determined at what point in its ATPase cycle myosin generates actin motion. Although these results were obtained from individual myosin motors, our analysis required the acquisition of many displacement events from a single motor. A more direct approach to determining the relationship between actomyosin ATPase biochemistry and mechanics is to simultaneously measure single fluorescent nucleotide binding and mechanical steps using a laser trap (Ishijima et al., 1998). We have also used a biochemically characterized myosin mutation to isolate the biochemistry of myosin's mechanical step. Additional selective mutations of the myosin molecule should allow us to further dissect the structural basis for myosin's mechanochemistry. Finally in this paper, we have used a model to compare the single-molecule mechanochemistry with that of an ensemble in a motility assay. To test this model further, the relationship between the actomyosin ATPase kinetics and ensemble motility will have to be directly measured by simultaneously detecting actin binding (Cooper et al., 2000), ATPase activity (Sowerby et al., 1993; Oiwa et al., 2000), and actin filament motility in an ensemble assay.

APPENDIX

In an effort to extract biochemical kinetics from actin filament velocities measured in the motility assay and to relate the actin filament movement generated by a single myosin molecule to that generated by an ensemble of myosin molecules, we develop a simple model of actin movement. Based on the literature, we assume that, in a laser trap, myosin generates actin filament motion with a discrete rotation of the myosin light chain domain, or neck, upon strong actin binding (Fig. 10 *a*). We refer to both the action and mechanism of the discrete displacement of an actin filament observed in a laser trap as a "mechanical step."

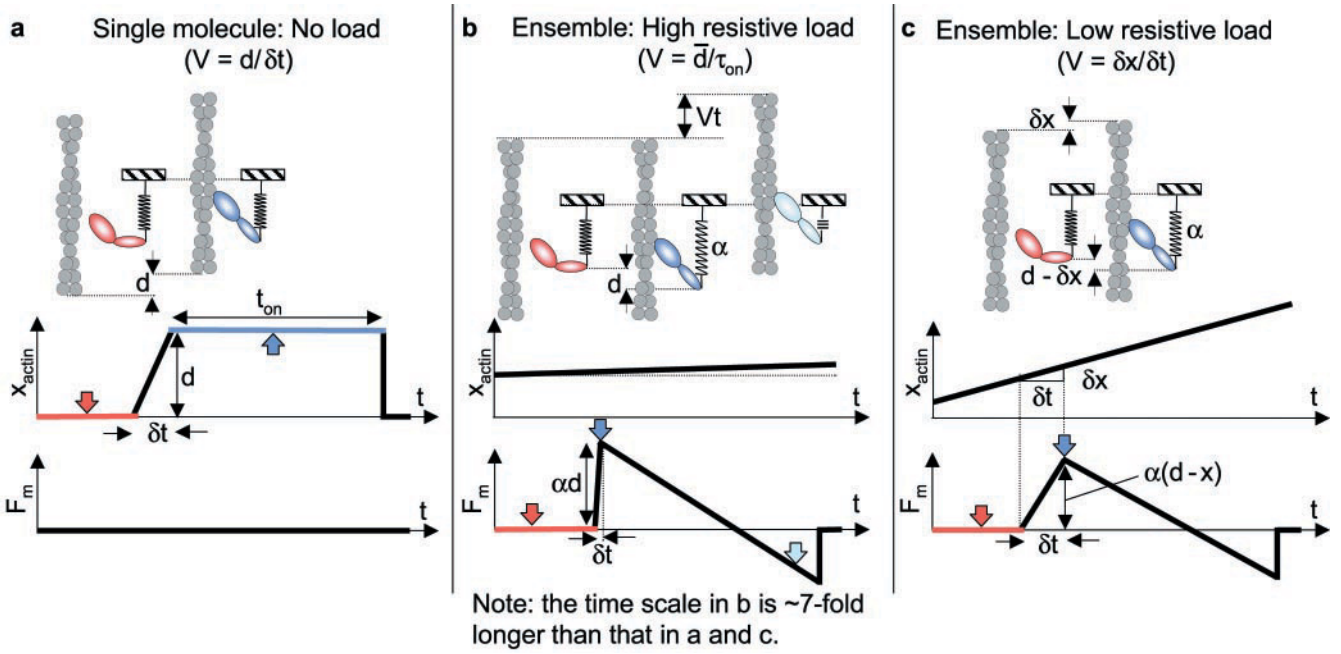

FIGURE 10 A model of actin movement. A hypothetical mechanism for the mechanical step is illustrated as a rotation of the myosin light chain domain when a myosin head (*ovals*) strongly binds to an actin filament (*helix*). The different myosin colors represent different biochemical/mechanical states: a weak binding state (*red*) and a strong binding state at various strains (*blues*). The degree of strain is illustrated by a spring-like element extending from the light chain domain. For the three cases presented, a hypothetical time course of the observable actin position (x) and the modeled force (F_m) of a given myosin motor is shown. For the unloaded, single molecule case (*a*), the measured actin position (x) provides a unique signature (color coded) of the actomyosin biochemical states, whereas for the loaded, ensemble cases (*b* and *c*), the biochemistry underlying actin filament movement must be modeled. (*a*) A mechanical step against no load is fully realized as actin movement and displaces an actin filament a distance d over the period δt at a velocity $d/\delta t$. The myosin force (F_m) remains zero during a mechanical step against zero load. However, in an actual laser-trap experiment, the myosin force probably spikes with a step, due to viscous drag, and then decays over the period δt to a value equal to the force exerted by the laser trap (estimated in our experiments to be ~0.4 pN for $d = 10$ nm). The unloaded case probably best applies to actin and myosin in solution. (*b*) If, in an ensemble motility experiment, an actin filament moves at a velocity, V, that is much less than $d/\delta t$, then a mechanical step can occur if it stretches a compliant element of stiffness α a distance d. The color-coded actomyosin states (*top*) and the corresponding color-coded arrows on the force traces (*bottom*) illustrate the proposed temporal relationship between actomyosin biochemistry and mechanics. In the Appendix, we show that, for this case, under rate-limiting conditions, the velocity is $V = \bar{d}/\tau_{on}$. In this model, force generation, which is associated with attachment kinetics, and actin movement, which is associated with detachment kinetics, occur on different time scales. To illustrate this, we had to make the time scale in (*b*) approximately 7-fold longer than the time scales in (*a*) and (*c*). (*c*) If a mechanical step is partitioned between moving an actin filament a distance δx and stretching the compliant element a distance $d - \delta x$, then the velocity is $V = \delta x/\delta t$ (see Appendix, Case 3). Once again, the color-coded actomyosin states (*top*) and the corresponding color-coded arrows on the force traces (*bottom*) illustrate the proposed temporal relationship between actomyosin biochemistry and mechanics.

Case 1: Unloaded mechanical step (e.g., single myosin molecule in a laser trap)

Figure 10 *a* illustrates the time course for our model of a mechanical step against zero load. We use this model to describe mechanical steps in a laser trap, which occur against a minimal load (see Fig. 10, legend), but this model (perhaps more aptly) also applies to mechanical steps in solution, which occur against a lower, largely viscous, load. In a laser trap assay, a single myosin molecule displaces an actin filament a distance d (~10 nm) over a period δt (<2 ms) that is shorter than the time resolution of our detection system. Thus during this period, the actin filament moves at a relatively high velocity ($V = d/\delta t > 5$ μm sec^{-1}). On the basis of data presented in this paper, three processes occur over the period, δt, of the mechanical step: myosin forms stereospecific (strong) bonds with actin; P_i dissociates from myosin (k_{Pi} in Fig. 1); and myosin moves an actin filament. For this unloaded case, actin velocities depend on the lifetime, δt, of the processes that displace an actin filament. In contrast, for the following case, we show that actin velocities depend on the lifetime, τ_{on}, of the processes that follow the step and precede detachment (i.e., ADP release and ATP binding).

Case 2: Mechanical step against a high resistive load (myosin ensemble in a motility assay)

In contrast to the unloaded case (case 1), if a high resistive load fully prevents an actin filament from moving, then the mechanical step generated by a single myosin molecule can occur if there is compliance in the actomyosin system. In Fig. 10 *b*, we illustrate a light chain domain rotation that stretches a compliant element of linear stiffness α, a distance d, generating a force αd. If the actin filament is subsequently allowed to move, the mechanism of motion generation is, in this case, the relaxation of the compliant element, not, as in case 1, the mechanical step itself.

Similar models, in which force generation precedes motion generation, have been used to describe the actin movement generated by an ensemble of myosin molecules (Huxley, 1957; Hill, 1974). A basic assumption of these models is that actin-attached myosin molecules in an ensemble impose a large resistive load that limits actin movement (Huxley, 1990; Spudich, 1994) and fully restricts the action of the mechanical step to force, not motion, generation. We calculate the actin filament velocity for this model by following a balanced force approach similar to that used in previous models (Huxley, 1957), only here we consider the stochastic

distribution of attachment times evident in our single-molecule experiments.

We begin by assuming that the actin filament in a motility assay moves at a constant velocity, V, that is much less than the actin velocity, $d/\delta t$, generated by a mechanical step against zero load (see case 1). In this case, the mechanical step generates an initial force of αd that decreases with time (Fig. 10 *b*, *lower trace*) as $F(t) = \alpha(d - Vt)$. The net work performed by the relaxation of the compliant element associated with a given myosin head during its attachment time, t_{on}, is

$$W = V\int_0^{t_{on}} F(t)\,\mathrm{d}t$$

$$= \alpha V\int_0^{t_{on}} (d - Vt)\,\mathrm{d}t$$

$$= \alpha V\left(dt_{on} - \frac{1}{2}Vt_{on}^2\right).$$

In an ensemble of myosin molecules with distributed steps of average size $\bar{d}$ and stochastically weighted attachment times, $n_{on}(t)$, the average work performed by a myosin head during its attachment time is

$$\bar{W} = \frac{\alpha V}{A}\int_0^{\infty}\left(\bar{d}t - \frac{1}{2}Vt^2\right)n_{on}(t)\,\mathrm{d}t.$$

Setting this equation equal to zero (on average, no net work is performed in a motility assay) and solving, using $n_{on}(t)$ from Eq. 3, we obtain the following expression for the dependence of V on both [ATP] and [ADP]:

$$\frac{\bar{d}}{V} = \frac{\dfrac{1}{(q-p)^3} - \dfrac{1}{(p+q)^3}}{\dfrac{1}{(p+q)^2} - \dfrac{1}{(q-p)^2}}, \qquad \text{(A1)}$$

where p and q are defined as for Eq. 1. We note that, because the detachment kinetics described by $n_{on}(t)$ in Eq. 3 are strain (x) independent, there is no inherent strain dependence in Eq. A1. However, strain dependence can be incorporated into this model by defining $n_{on}(t, x)$.

For [ADP] = 0, Eq. A1 reduces to

$$\frac{\bar{d}}{V} = \frac{\dfrac{1}{k_{-D}^3} - \dfrac{1}{(k_T[ATP])^3}}{\dfrac{1}{k_{-D}^2} - \dfrac{1}{(k_T[ATP])^2}}, \qquad \text{(A2)}$$

and, if a single biochemical step limits detachment, Eq. A2 can be further simplified to

$$\frac{\bar{d}}{V} = \frac{1}{k_{rls}} = \tau_{on}, \qquad \text{(A3)}$$

where k_{rls} is k_{-D} at sufficiently high [ATP] (i.e., $k_T[ATP] \gg k_{-D}$) and k_{rls} is $k_T[ATP]$ at sufficiently low [ATP] (i.e., $k_T[ATP] \ll k_{-D}$).

This equation (Eq. A3) is frequently used as a first approximation to relate actin filament velocities (V) measured in a motility assay to the mechanical ($\bar{d}$) and kinetic (τ_{on}) properties of individual myosin molecules (Huxley, 1990; Spudich, 1994). Here we have formally established two critical assumptions behind this equation: attached myosin heads impose a resistive load that completely prevents mechanical steps from being realized as actin movement, and detachment rates are independent of strain. According to Eq. A3, both actin filament velocities, V, and single-molecule τ_{on} values should exhibit the same dependence on [ATP]. In other words, $K_{M(on)}$ in Eq. 5 should be equal to $K_{M(vel)}$ in Eq. 6. The factor of five difference observed between $K_{M(on)}$ and $K_{M(vel)}$ (see Results) implies that at least one of the above assumptions of this model does not apply to our motility data over all ATP concentrations.

In Fig. 10, we place the compliant element distal to the lever arm (perhaps corresponding to the S2 region) as originally proposed by Huxley and Simmons (1971). This is necessary to explain studies indicating that a large and discrete rotation of the light chain domain occurs even against relatively high loads (Van Buren et al., 1994; Baker et al., 1998). However, other studies indicate that the compliance is located elsewhere (Huxley, 1969; Howard and Spudich, 1996; Irving et al., 2000), and it may in fact be that compliant points are distributed throughout the myosin molecule. Nevertheless, the exact location of the compliant element does not affect the predicted relationships above. For instance, Eq. A3 is also derived for a torque motor that, upon strong actin binding, generates torque—not a light chain domain rotation—within a compliant element located between the motor and light chain domains (Huxley, 1969; Houdusse and Sweeney, 2001). One exception, however, is that, if compliant elements mechanically couple myosin motors in the ensemble (e.g., through the actin filament) $F(t)$ for a given myosin head is not well defined and actin velocities must be determined using stochastic simulations or a mean field approach (Baker and Thomas, 2000).

Although both models described above (case 1 and case 2) share a rotating lever arm as a common feature, each case has actin filament motion resulting from a different mechanism associated with a different biochemical step in the actomyosin ATPase cycle. In the unloaded case (case 1), the mechanism of motion generation is the lever arm rotation itself, which is associated with attachment kinetics. In the high load case (case 2), the mechanism of motion generation is the relaxation of a strained mechanical element, which is limited by detachment kinetics.

Case 3: Mechanical step against an intermediate resistive load

In the unloaded case (case 1), a mechanical step, during the period of the step δt, moves an actin filament a distance d but does not generate force. Whereas in the high load case (case 2), a mechanical step, during the period of the step δt, generates a force αd but does not move an actin filament. These two cases represent two extreme limits of a more general, intermediate model in which a mechanical step, over the period of the step δt, is partitioned between moving an actin filament a distance δx and stretching compliant elements a distance $d - \delta x$ (Fig. 10 *c*). Because the actin filament moves a distance δx during the period δt, its velocity is $V = \delta x/\delta t$. The period δt, as in case 1, is related to attachment kinetics, and the distance the actin moves, δx, is influenced by the forces that resist the action of the mechanical step. Veigel et al. (1998) derived an expression for δx as a function of the stiffness of the various compliant elements in a single-molecule actomyosin system. Here we derive an expression for δx as a function of the net resistive load of the attached heads in an ensemble motility system.

Unlike in case 1, here the average work performed on a given attached myosin head is not equal to zero but is balanced by the work performed by the mechanical steps of other myosin heads. Thus the balanced-force approach used in the previous case does not apply here. The simplest alternative is to consider that, at a constant actin filament velocity, V, a mechanical step performs work against the net resistive load, F, of the attached myosin heads. Here F is a phenomenological parameter that is proportional to the number of strongly bound myosin heads (and the strength and number of weak interactions). We can then obtain an expres-

sion for the sliding velocity, V, using a macroscopic approach, such as Hill's force:velocity relationship (Hill, 1938),

$$V = (F_{max} - F)b/(aF_{max} + F).$$

Baker and Thomas (2000) showed that $F_{max}\bar{d}$ is related to the free energy of the mechanical step, and that the parameters a and b are related to the step duration, δt, the mean step size, $\bar{d}$, and the reaction cycle time (the inverse ATPase rate), τ_{cycle}, as $a = \delta t/\tau_{cycle}$ and $b = \bar{d}/\tau_{cycle}$. Substituting $V = \delta x/\delta t$ and the above expressions for a and b into the force:velocity equation, we obtain an expression for the fraction of the mechanical step realized as motion,

$$\delta x/\bar{d} = \{F_{max} - F\}/\{F_{max} + (\tau_{cycle}/\delta t)F\}.$$

This equation unites the three cases presented in this appendix. If the net resistive force, F, of the attached myosin heads equals the net driving force, F_{max}, of the mechanical steps, then the above equation predicts that $\delta x = 0$. This is the loaded limit (case 2) for which we showed that $V \sim \bar{d}/t_{on}$. At the other extreme, if there is no resistive force ($F = 0$), then the above equation predicts that $\delta x = \bar{d}$. This is the unloaded limit (case 1) for which we showed that $V = \bar{d}/\delta t$. At intermediate F values ($0 \le F \le F_0$), the above equation predicts that δx has a value between 0 and $\bar{d}$. This is the intermediate case (case 3) for which the actin filament moves a distance δx during the period of the mechanical step, δt, at a velocity $V = \delta x/\delta t = \bar{d}\{F_{max} - F\}/\{\delta t F_{max} + t_c F\}$.

The models presented above imply that the maximum velocity at which a myosin molecule can move an actin filament is $V = d/\delta t$ (case 1). This velocity can be maintained by a single myosin molecule for only a short period of time, δt, and could be sustained by an ensemble of myosin molecules if attached heads offered no resistance to actin movement (Baker and Thomas, 2000). However, in a motility assay, attached heads probably do resist actin movement, with an increased number of attached heads increasing resistance and decreasing the velocity below the maximum value of $d/\delta t$, until the velocity reaches a detachment-limited value of $V = \bar{d}/t_{on}$. But is the fraction of attached heads in a motility assay sufficient to reach this detachment limit? At low [ATP] a large fraction of myosin molecules are attached to actin, and we observe that the actin velocity is indeed limited by detachment kinetics. As the ATP concentration is increased, however, the fraction of attached heads decreases, and we observe that, at [ATP] $> 100\ \mu$M, actin velocities deviate from detachment limited kinetics, indicating that the relatively small fraction of actin-attached heads at these low ATP concentrations might not be sufficient to fully limit actin velocities.

We thank K. Trybus for her support in providing us with the smooth muscle myosin mutant. We thank J. Patlak and J. Moore for helpful discussions. We thank G. Kennedy and E. Hayes for technical assistance. Finally, we thank B. Palmer for his contributions to our modeling efforts.

This study was funded by grants from the National Institutes of Health to J.E.B. (HL07647) and D.M.W. (AR47906, HL59408).

REFERENCES

Anson, M., M. A. Geeves, S. E. Kurzawa, and D. J. Manstein. 1996. Myosin motors with artificial lever arms. *EMBO J.* 15:6069–6074.

Baker, J. E., I. Brust-Mascher, S. Ramachandran, L. E. W. LaConte, and D. D. Thomas. 1998. A large and distinct rotation of the myosin light chain domain occurs upon muscle contraction. *Proc. Natl. Acad. Sci. U.S.A.* 95:2944–2949.

Baker, J. E., and D. D. Thomas. 2000. A Thermodynamic muscle model and a chemical basis for A. V. Hill's muscle equation. *J. Muscle Res. Cell Motil.* 21:335–344.

Barany, M. 1967. ATPase activity correlated with speed of muscle shortening. *J. Gen. Physiol.* 50:197–218.

Cooke, R. 1997. Actomyosin interaction in striated muscle. *Physiol. Rev.* 77:671–697.

Cooke, R., and W. Bialek. 1979. Contraction of glycerinated muscle fibers as a function of the ATP concentration. *Biophys. J.* 28:241–258.

Cooper, W. C., L. R. Chrin, and C. L. Berger. 2000. Detection of fluorescently labeled actin-bound cross-bridges in actively contracting myofibrils. *Biophys. J.* 78:1449–1457.

Dantzig, J. A., M. G. Hibberd, D. R. Trentham, and Y. E. Goldman. 1991. Cross-bridge kinetics in the presence of MgADP investigated by photolysis of caged ATP in rabbit psoas muscle fibres. *J. Physiol.* 432: 639–680.

Dantzig, J. A., Y. E. Goldman, N. C. Millar, J. Lacktis, and E. Homsher. 1992. Reversal of the cross-bridge force-generating transition by photogeneration of phosphate in rabbit psoas muscle fibres. *J. Physiol. Lond.* 451:247–278.

Dominguez, R., Y. Freyzon, K. M. Trybus, and C. Cohen. 1998. Crystal structure of a vertebrate smooth muscle myosin motor domain and its complex with the essential light chain: visualization of the pre-power stroke state. *Cell.* 94:559–571.

Dupuis, D. E., W. Guilford, J. Wu, and D. M. Warshaw. 1997. Actin filament mechanics in the laser trap. *J. Muscle Res. Cell Motil.* 18: 17–30.

Eisenberg, E., and T. L. Hill. 1985. Muscle contraction and free energy transduction in biological systems. *Science.* 227:999–1006.

Fabiato, A., and F. Fabiato. 1979. Calculator programs for computing the composition of the solutions containing multiple metals and ligand used for experiments in skinned muscle cells. *J. Physiol. (Paris).* 75:463–505.

Finer, J. T., R. M. Simmons, and J. A. Spudich. 1994. Single myosin molecule mechanics: piconewton forces and nanometer steps. *Nature.* 368:113–119.

Fortune, N. S., M. A. Geeves, and K. W. Ranatunga. 1991. Tension responses to rapid pressure release in glycerinated rabbit muscle fibers. *Proc. Natl. Acad. Sci. U.S.A.* 88:7323–7327.

Geeves, M. A. 1989. Dynamic interaction between actin and myosin subfragment 1 in the presence of ADP. *Biochemistry.* 28:5864–5871.

Goldman, Y. E. 1987. Kinetics of the actomyosin ATPase in muscle fibers. *Ann. Rev. Physiol.* 49:637–654.

Guilford, W. H., D. E. Dupuis, G. Kennedy, J. Wu, J. B. Patlak, and D. M. Warshaw. 1997. Smooth muscle and skeletal muscle myosins produce similar unitary forces and displacements in the laser trap. *Biophys. J.* 72:1006–1021.

Harris, D. E., and D. M. Warshaw. 1993. Smooth and skeletal myosin duty cycle in vitro. *J. Biol. Chem.* 268:14764–14768.

Hill, A. V. 1938. The heat of shortening and the dynamic constants of muscle. *Proc. R. Soc. Lond. Ser. B.* 126:136–195.

Hill, T. L. 1974. Theoretical formalism for the sliding filament model of contraction of striated muscle. Part I. *Prog. Biophys. Molec. Biol.* 28:267–340.

Houdusse, A., and H. L. Sweeney. 2001. Myosin motors: missing structures and hidden springs. *Curr. Opin. Struct. Biol.* 11:182–194.

Houdusse, A., A. G. Szent-Gyorgyi, and C. Cohen. 2000. Three conformational states of scallop myosin S1. *Proc. Natl. Acad. Sci. U.S.A.* 97:11238–11243.

Homsher, E., F. Wang, and J. R. Sellers. 1993. Factors affecting movement of F-actin filaments propelled by skeletal muscle heavy meromyosin. *Adv. Exp. Med. Biol.* 332:279–289.

Howard, J., and J. A. Spudich. 1996. Is the lever arm of myosin a molecular elastic element? *Proc. Natl. Acad. Sci. U.S.A.* 93:4462–4464.

Huxley, A. F. 1957. Muscle structure and theories of contraction. *Prog. Biophys.* 7:255–317.

Huxley, A. F., and R. M. Simmons. 1971. Proposed mechanism of force generation in striated muscle. *Nature.* 233:533–538.

Huxley, H. E. 1969. The mechanism of muscular contraction. *Science.* 164:1356–1366.

Huxley, H. E. 1990. Sliding filaments and molecular motile systems. *J. Biol. Chem.* 265:8347–8350.

Irving, M., G. Piazzesi, L. Lucii, Y. B. Sun, J. J. Harford, I. M. Dobbie, M. A. Ferenczi, M. Reconditi, and V. Lombardi. 2000. Conformation of the myosin motor during force generation in skeletal muscle. *Nat. Struct. Biol.* 7:482–485.

Irving, M., T. St. Claire Allen, C. Sabido-David, J. S. Craik, B. Brandmeier, J. Kendrick-Jones, J. E. Corrie, D. R. Trentham, and Y. E. Goldman. 1995. Tilting of the light-chain region of myosin during step length changes and active force generation in skeletal muscle. *Nature.* 375:688–691.

Ishijima, A., H. Kojima, T. Funatsu, M. Tokunaga, H. Higuchi, H. Tanaka, and T. Yanagida. 1998. Simultaneous observation of individual ATPase and mechanical events by a single myosin molecule during interaction with actin. *Cell.* 92:161–171.

Joel, P. B., K. M. Trybus, and H. L. Sweeney. 2001. Two conserved lysines at the 50/20-kDa junction of myosin are necessary for triggering actin activation. *J. Biol. Chem.* 276:2998–3003.

Kawai, M., and H. R. Halvorson. 1991. Two step mechanism of phosphate release and the mechanism of force generation in chemically skinned fibers of rabbit psoas muscle. *Biophys. J.* 59:329–342.

Lauzon, A. M., M. J. Tyska, A. S. Rovner, Y. Freyzon, D. M. Warshaw, and K. M. Trybus. 1998. A 7-amino-acid insert in the heavy chain nucleotide binding loop alters the kinetics of smooth muscle myosin in the laser trap. *J. Muscle Res. Cell Motil.* 19:825–837.

Linari, M., G. Piazzesi, I. Dobbie, N. Koubassova, M. Reconditi, T. Narayanan, O. Diat, M. Irving M, and V. Lombardi. 2000. Interference fine structure and sarcomere length dependence of the axial x-ray pattern from active single muscle fibers. *Proc. Natl. Acad. Sci. U.S.A.* 97: 7226–7231.

Lu, H. P., L. Xun, and X. S. Xie. 1998. Single-molecule enzymatic dynamics. *Science.* 282:1877–1882.

Lymn, R. W., and E. W. Taylor. 1971. Mechanism of adenosine triphosphate hydrolysis by actomyosin. *Biochemistry.* 10:4617–4624.

Marston, S. B., and E. W. Taylor. 1980. Comparison of the myosin and actomyosin ATPase mechanisms of the four types of vertebrate muscles. *J. Mol. Biol.* 139:573–600.

Molloy, J. E., J. E. Burns, J. Kendrick-Jones, R. T. Tregear, and D. C. S. White. 1995. Movement and force produced by a single myosin head. *Nature.* 378:209–212.

Oiwa, K., J. F. Eccleston, M. Anson, M. Kikumoto, C. T. Davis, G. P. Reid, M. A. Ferenczi, J. E. Corrie, A. Yamada, H. Nakayama, and D. R. Trentham. 2000. Comparative single-molecule and ensemble myosin enzymology: sulfoindocyanine ATP and ADP derivatives. *Biophys. J.* 78:3048–3071.

Palmiter, K. A., M. J. Tyska, D. E. Dupuis, N. R. Alpert, and D. M. Warshaw. 1999. Kinetic differences at the single molecule level account for the functional diversity of rabbit cardiac myosin isoforms. *J. Physiol.* 519:669–678.

Palmiter, K. A., M. J. Tyska, J. R. Haeberle, N. R. Alpert, L. Fananapazir, and D. M. Warshaw. 2000. R403Q and L908V mutant beta-cardiac myosin from patients with familial hypertrophic cardiomyopathy exhibit enhanced mechanical performance at the single molecule level. *J. Muscle Res. Cell Motil.* 21:609–620.

Pardee, J. D., and J. A. Spudich. 1982. Purification of muscle actin. *Methods Enzymol.* 85:164–181.

Patlak, J. B. 1993. Measuring kinetics of complex single ion channel data using mean-variance histograms. *Biophys. J.* 65:29–42.

Ranatunga, K. W. 1999. Effects of inorganic phosphate on endothermic force generation in muscle. *Proc. R. Soc. Lond. B. Biol. Sci.* 266: 1381–1385.

Rayment, I., W. R. Rypniewski, K. Schmidt-Base, R. Smith, D. R. Tomchick, M. M. Benning, D. A. Winkelmann, G. Wesenberg, and H. M. Holden. 1993. Three-dimensional structure of myosin subfragment-1; a molecular motor. *Science.* 261:50–65.

Reedy, M. K., K. C. Holmes, and R. T. Tregear. 1965. Induced changes in orientation of the cross-bridges of glycerinated insect flight muscle. *Nature.* 297:1276–1280.

Ruff, C., M. Furch, B. Brenner, D. J. Manstein, and E. Meyhofer. 2001. Single-molecule tracking of myosins with genetically engineered amplifier domains. *Nat. Struct. Biol.* 8:226–229.

Sellers, J. R. 1999. Myosins. 2nd edition. Oxford University Press, Oxford, U.K.

Siemankowski, R. F., M. O. Wiseman, and H. D. White. 1985. ADP dissociation from actomyosin subfragment 1 is sufficiently slow to limit the unloaded shortening velocity in vertebrate muscle. *Proc. Natl. Acad. Sci. U.S.A.* 82:658–662.

Sleep, J. A., and R. L. Hutton. 1980. Exchange between inorganic phosphate and adenosine 5′-triphosphate in the medium by actomyosin subfragment 1. *Biochemistry.* 19:1276–1283.

Sowerby, A. J., C. K. Seehra, M. Lee, and C. R. Bagshaw. 1993. Turnover of fluorescent nucleoside triphosphates by isolated immobilized myosin filaments. Transient kinetics on the zeptomole scale. *J. Mol. Biol.* 234:114–123.

Spudich, J. A. 1994. How molecular motors work. *Nature.* 372:515–518.

Taylor, K. A., H. Schmitz, M. C. Reedy, Y. E. Goldman, C. Franzini-Armstrong, H. Sasaki, R. T. Tregear, K. Poole, C. Lucaveche, R. J. Edwards, L. F. Chen, H. Winkler, and M. K. Reedy. 1999. Tomographic 3D reconstruction of quick-frozen, Ca^{2+}-activated contracting insect flight muscle. *Cell.* 99:421–431.

Trybus, K. M., and L. Henry. 1989. Monoclonal antibodies detect and stabilize conformational states of smooth muscle myosin. *J. Cell Biol.* 109:2879–2886.

Tyska, M. J., and D. M. Warshaw. 2002. The myosin power stroke. *Cell Motil. Cytoskeleton*. 51:1–15.

Uyeda, T. Q., P. D. Abramson, and J. A. Spudich. 1996. The neck region of the myosin motor domain acts as a lever arm to generate movement. *Proc. Natl. Acad. Sci. U.S.A.* 93:4459–4464.

Van Buren, P., G. S. Waller, D. E. Harris, K. M. Trybus, D. M. Warshaw, and S. Lowey. 1994. The essential light chain is required for full force production by skeletal muscle myosin. *Proc. Natl. Acad. Sci. U.S.A.* 91:12403–12407.

Veigel, C., M. L. Bartoo, D. C. White, J. C. Sparrow, and J. E. Molloy. 1998. The stiffness of rabbit skeletal actomyosin cross-bridges determined with an optical tweezers transducer. *Biophys. J.* 75:1424–1438.

Walker, J. W., Z. Lu, and R. L. Moss. 1992. Effects of Ca^{2+} on the kinetics of phosphate release in skeletal muscle. *J. Biol. Chem.* 267:2459–2466.

Walker, M., X. Z. Zhang, W. Jiang, J. Trinick, and H. D. White. 1999. Observation of transient disorder during myosin subfragment-1 binding to actin by stopped-flow fluorescence and millisecond time resolution electron cryomicroscopy: evidence that the start of the crossbridge power stroke in muscle has variable geometry. *Proc. Natl. Acad. Sci. U.S.A.* 96:465–470.

Warshaw, D. M., J. M. Desrosiers, S. S. Work, and K. M. Trybus. 1990. Smooth muscle myosin cross-bridge interactions modulate actin filament sliding velocity in vitro. *J. Cell Biol.* 111:453–463.

Warshaw, D. M., E. Hayes, D. Gaffney, A. M. Lauzon, J. Wu, G. Kennedy, K. M. Trybus, S. Lowey, and C. Berger. 1998. Myosin conformational states determined by single fluorophore polarization. *Proc. Natl. Acad. Sci. U.S.A.* 95:8034–8039.

Warshaw, D. M., W. H. Guilford, Y. Freyzon, E. Krementsova, K. A. Palmiter, M. J. Tyska, J. E. Baker, and K. M. Trybus. 2000. The light chain binding domain of expressed smooth muscle heavy meromyosin acts as a mechanical lever. *J. Biol. Chem.* 275:37165–37172.

Weiss, S., R. Rossi, M. A. Pellegrino, R. Bottinelli, and M. A. Geeves. 2001. Differing ADP release rates from myosin heavy chain isoforms define the shortening velocity of skeletal muscle fibers. *J. Biol. Chem.* 276:45902–45908.

White, H. D., and E. W. Taylor. 1976. Energetics and mechanism of actomyosin adenosine triphosphatase. *Biochemistry.* 15:5818–5826.